Primordial black hole abundance from the power spectrum of cosmological perturbations

Author: Matteo Gabriel Marrone, mmarroma10@alumnes.ub.edu
Facultat de Física, Universitat de Barcelona, Diagonal 645, 08028 Barcelona, Spain.

Advisor: Jaume Garriga Torres, jgarriga@fqa.ub.edu

Abstract: A random field of cosmological perturbations may have rare high peaks which evolve non-linearly after they cross the horizon during the radiation dominated era, forming primordial black holes (PBH). Using recent results for the statistics of large initial overdensities, we will consider a family of well motivated profiles for such overdensities, determining the critical amplitude which causes them to collapse gravitationally. This is relevant for determining the abundance of PBH for a given primordial power spectrum of cosmological perturbations.
Keywords: Cosmology, primordial perturbations, gravitational collapse, black holes.
SDGs: This work is related to the sustainable-development goal (SDG) "quality education" (see page 6).

I. INTRODUCTION

Primordial black holes (PBH) may have formed from the collapse of rare high density peaks during the radiation dominated epoch [1]. They are a promising dark matter candidate, particularly in the asteroid mass range, $M \in [10^{17}\text{g}, 10^{23}\text{g}]$. Such scenarios are currently under active investigation, see e.g. [2] for a recent review and a summary of observational constraints.

Here we elaborate on a recent approach to finding the mass function of PBH starting from the power spectrum of primordial cosmological perturbations [3]. In Section II we will present the Misner-Sharp equations, describing spherically symmetric gravitational collapse of a perfect fluid. We comment on the initial conditions for numerical evolution in Section III. In Sections IV we introduce the compaction function, which is a useful tool for characterizing overdensities. In Section V we will introduce a one parameter family of profiles for the overdensities which will be of particular relevance in our context. We also introduce a specific form of the power spectrum, suitably enhanced within a range of scales so as to give a relevant abundance of PBH. In section VI we will present the numerical results for the threshold values of critical collapse, for our chosen family of profiles. In Section VII we calculate the abundance of PBH, by integrating over the Gaussian random field of initial perturbations, comparing our results with the approach recently presented in [3]. We summarize or conclusions in Section VIII.

II. MISNER-SHARP EQUATIONS

The Misner-Sharp equations [4] are a set of relativistic differential equations describing a spherically symmetric perfect fluid undergoing gravitational collapse. We will apply these equations to the cosmological context, within a Friedmann-Lemaitre-Robertson-Walker (FLRW) background. We consider the energy-momentum tensor of a perfect fluid to be $T^{\mu\nu} = (p+\rho)u^\mu u^\nu + pg^{\mu\nu}$, where p and ρ are the pressure and energy density of the fluid, respectively. They are related by the equation of state $p = w\rho$, where $w = 1/3$ in a radiation dominated Universe. The line element is given by,

$$ds^2 = -A(r,t)^2dt^2 + B(r,t)^2dr^2 + R(r,t)^2d\Omega^2, \quad (1)$$

where $d\Omega^2 = d\theta^2 + \sin^2\theta d\varphi^2$ is the metric on the unit 2-sphere, and $R(r,t)$ the areal radius. The Misner-Sharp mass is defined as,

$$M(r,t) \equiv \int_0^R 4\pi R^2 \rho \left(\frac{\partial R}{\partial r}\right) dr, \quad (2)$$

and satisfies the following equality,

$$\Gamma = \sqrt{1 + U^2 - \frac{2M}{R}}, \quad (3)$$

where we have introduced

$$U \equiv D_t R = \frac{1}{A}\frac{\partial R}{\partial t}, \quad \Gamma \equiv D_r R = \frac{1}{B}\frac{\partial R}{\partial r}. \quad (4)$$

The Misner-Sharp (MS) equations can be expressed in the following manner [5],

$$\dot{U} = -A\left(\frac{w}{1+w}\frac{\Gamma^2}{\rho}\frac{\rho'}{R'} + \frac{M}{R^2} + 4\pi R w\rho\right), \quad (5a)$$

$$\dot{R} = AU, \quad (5b)$$

$$\dot{\rho} = -A\rho(1+w)\left(2\frac{U}{R} + \frac{U'}{R'}\right), \quad (5c)$$

$$\dot{M} = -4\pi A w\rho U R^2, \quad (5d)$$

$$M' = 4\pi R^2 \rho R', \quad (5e)$$

$$A' = -A\frac{w}{1+w}\frac{\rho'}{\rho} \Longrightarrow A(r,t) = \left(\frac{\rho_b(t)}{\rho(r,t)}\right)^{\frac{w}{w+1}}. \quad (5f)$$

Here, $\rho_b(t) = \rho_0(t_0/t)^2$ is the energy density of the FLRW background, and $\rho_0 = 3H_0^2/8\pi$. Note that we used the

boundary condition $A(r \to \infty, t) = 1$ so that we recover FLRW at large r. For reference, we recall that the expansion rate is given by $H(t) = H_0 t_0/t$ and the scale factor in the radiation era is given by $a(t) \propto \sqrt{t}$.

The set of equations (5) will be solved using the public numerical code developed by A. Escrivà (see [5, 6] for a detailed discussion of the method). This is based on a pseudo-spectral Chebyshev collocation method for computing the spatial derivatives, while the time evolution is solved with a fourth-order Runge-Kutta method. Equation (5e) corresponds to the Hamiltonian constraint, which we can utilize to monitor the numerical accuracy of time evolution.

III. LONG WAVELENGTH APPROXIMATION

At early times, the characteristic lengthscale L of the cosmological density fluctuations can be considered to be much larger than the corresponding Hubble radius, $L \gg H^{-1}$. Within this regime, we can expand the exact solutions for the initial metric and hydrodynamic variables in powers of a dimensionless small parameter [5],

$$\epsilon(t) \equiv \frac{1}{H(t)L(t)} \ll 1. \tag{6}$$

In the limit where $\epsilon \to 0$, the perturbed FLRW metric reduces to

$$ds^2 = -dt^2 + a^2(t)e^{2\zeta(r)}(dr^2 + r^2 d\Omega^2), \tag{7}$$

where we have considered explicitly spherical symmetry, and where the function $\zeta(r)$ is the so-called gauge-invariant curvature perturbation, which is time independent in this limit. To lowest order, the long wavelength solution to the MS equations (5) can be expressed in the following way [7],

$$U = H(t)R(1 + \epsilon^2 \tilde{U}), \tag{8a}$$

$$\rho = \rho_b(t)(1 + \epsilon^2 \tilde{\rho}), \tag{8b}$$

$$M = \frac{4\pi}{3}\rho_b(t)R^3(1 + \epsilon^2 \tilde{M}), \tag{8c}$$

$$R = a(t)re^{\zeta(r)}(1 + \epsilon^2 \tilde{R}), \tag{8d}$$

where the tilde variables are defined as follows [7],

$$\tilde{U} = \frac{1}{5+3w}\frac{e^{2\zeta(r_m)}}{e^{2\zeta(r)}}\zeta'(r)\left(\frac{2}{r} + \zeta'(r)\right)r_m^2, \tag{9a}$$

$$\tilde{\rho} = -\frac{2(1+w)}{5+3w}\frac{e^{2\zeta(r_m)}}{e^{2\zeta(r)}}\left[\zeta''(r) + \zeta'(r)\left(\frac{2}{r} + \frac{\zeta'(r)}{2}\right)\right]r_m^2, \tag{9b}$$

$$\tilde{M} = -3(1+w)\tilde{U},\ \tilde{R} = -\frac{w}{(1+3w)(1+w)}\tilde{\rho} + \frac{\tilde{U}}{1+3w}. \tag{9c}$$

and where r_m is the comoving lengthscale of the perturbation, defined from $L(t) = a(t)r_m e^{\zeta(r_m)} = H^{-1}(t)/\epsilon$. Equations (8) will specify the initial conditions for numerical evolution of the MS equations, for a given initial perturbation $\zeta(r)$ (5).

IV. COMPACTION FUNCTION

A useful estimator to investigate PBH formation from the collapse of high density peaks is the so-called compaction function [8],

$$C(r,t) \equiv \frac{2(M - M_b)}{R} = \frac{2\delta M}{R}, \tag{10}$$

defined as the mass excess δM within a given R [9]. Within the long wavelength approximation, the value of the compaction function is time independent, given by,

$$C(r) = g(r)\left(1 - \frac{3}{8}g(r)\right), \tag{11}$$

where $g(r) = -\frac{4}{3}r\zeta'(r)$ [10]. From these definitions it can be seen that the super-horizon compaction function satisfies $C \leq 2/3$, with $g = 4/3$ saturating the inequality. This value separates fluctuations of Type I ($g < 4/3$) from Type II ($g > 4/3$), where the latter are characterized primarily by a non-monotonic behavior of the areal radius[1] as a function of r. Typical initial overdensities are weak, dissipating as sound waves once they fall within the horizon, without forming PBH's. However, for rare initial fluctuations, the maximum value of the compaction function at some scale $r = r_m$ may eventually grow to a large enough value $C(r_m, t) \approx 1$. By that time, a trapped surface with $2M/R > 1$ has formed, signaling the imminence of gravitational collapse and the formation of a PBH. Here we will be interested in studying the threshold values g_c (or C_c) above which a black hole will eventually form, and below which the overdensity dissipates, for different families of curvature profiles $\zeta(r)$.

V. CURVATURE PROFILE $\zeta(r)$

The curvature perturbation random field $\zeta(\mathbf{x})$ can be decomposed in its Fourier modes $\zeta_{\mathbf{k}}$,

$$\zeta(\mathbf{x}) = \int \frac{d^3\mathbf{k}}{(2\pi)^3} e^{i\mathbf{k}\cdot\mathbf{x}}\zeta_{\mathbf{k}}, \tag{12}$$

where here we consider $\zeta_{\mathbf{k}}$ to be Gaussian distributed, fully determined by the correlator $\langle \zeta_{\mathbf{k}}\zeta_{\mathbf{k}'}\rangle$, or equivalently

[1] This implies that, for some r, $R'(r) = 0$, and the set of equations (5) will be inadequate due to 0/0 indeterminacies. This is solved in [6] with a new approach where an additional auxiliary variable is introduced in the time evolution.

the dimensionless power spectrum $P_\zeta(k)$. Both are related by,

$$\langle \zeta_{\mathbf{k}} \zeta_{\mathbf{k}'} \rangle = (2\pi)^3 \delta^{(3)}(\mathbf{k}+\mathbf{k}') \frac{2\pi^2}{k^3} P_\zeta(k). \tag{13}$$

The power spectrum represents the variance of the random field per logarithmic interval in k,

$$\langle \zeta^2 \rangle = \int \frac{dk}{k} P_\zeta(k) = \int P_\zeta(k) d\log k. \tag{14}$$

For instance, the mean profile conditioned to a given value μ at the origin is given by [9, 11],

$$\zeta_{\rm mean}(r) = \mu \frac{\langle \zeta(r)\zeta(0)\rangle}{\langle \zeta^2 \rangle} = \frac{\mu}{\langle \zeta^2 \rangle} \int \frac{dk}{k} \mathrm{sinc}(kr) P_\zeta(k). \tag{15}$$

Here, instead, we will consider a one parameter family of profiles which is motivated by the optimization of the estimator $g(r)$, whose relevance will be discussed in Section VII. The mean profile conditioned to a large value of $g > g_c \sim 1$ at a certain scale r_m (which is the free parameter), and normalized to the value μ at the origin, is given by

$$\zeta_{\rm mean}(r; r_m) \equiv \mu \frac{\langle \zeta(r) g(r_m)\rangle}{\langle \zeta(0) g(r_m)\rangle} \tag{16a}$$

$$\propto \mu \int \frac{dk}{k} P_\zeta(k) \frac{\sin kr}{kr} \left(\frac{\sin kr_m}{kr_m} - \cos kr_m \right). \tag{16b}$$

For definiteness, we consider a nearly scale-invariant enhancement in the primordial power spectrum, between an infrared scale $k_{\rm IR}$ and an ultraviolet scale $k_{\rm UV}$,

$$P_\zeta(k) = A_s \Theta(k - k_{\rm IR}) \Theta(k_{\rm UV} - k). \tag{17}$$

With $A_s \sim 0.01$, this leads to a significant abundance of PBH. We note that $\zeta_{\rm mean} \sim 1$, while typical deviations from the mean profile are small, of order $A_s^{1/2} \sim 0.1$.

VI. THRESHOLDS

Before presenting the numerical results for the threshold values $g_c(r_m)$ in the family of profiles (16b), we briefly outline the so called "q-approach" introduced in [12]. This provides an estimate of the threshold based on the behavior of the *initial* compaction function near its maximum [10], by considering a fiducial fitting function [12],

$$C_{\rm fit}(r) = C(r_m) \frac{r^2}{r_m^2} e^{\frac{1}{q}(1 - r^{2q}/r_m^{2q})}. \tag{18}$$

This has a maximum at $r = r_m$ with normalized curvature $q \equiv -r_m^2 C''(r_m)/[4C(r_m)(1 - 3C(r_m)/2)]$. It also has the standard properties of decaying to 0 at sufficiently large r and having a r^2 dependence near the origin. The average of this fitting function,

$$\bar{C}(r) \equiv \frac{3}{r_m^3} \Theta(r - r_m) \int_0^{r_m} C_{\rm fit}(r') r'^2 dr', \tag{19}$$

can be used to infer the fate of the perturbation. Interestingly, for the case of a radiation dominated Universe, gravitational collapse will occur (approximately) for $\bar{C} \geq \bar{C}_c \equiv \frac{2}{5}$, independently of q [12]. By inverting (19) and taking advantage of this universality, one obtains that the critical value of the original compaction function, C_c, is of the form,

$$C_c(q) = \frac{4}{15} e^{-\frac{1}{q}} \frac{q^{1-\frac{5}{2q}}}{\Gamma(\frac{5}{2q}) - \Gamma(\frac{5}{2q}, \frac{1}{q})}, \tag{20}$$

where $\Gamma(x)$ and $\Gamma(x,y)$ are the Euler gamma and upper-incomplete gamma functions, respectively. This expression predicts a lower bound given by $C_c \geq 2/5$, and a saturating value of $C_c = \frac{2}{3}$ in the large q limit, i.e. the threshold value will remain in the Type I region. Expression (20) has been tested [12] in the low $q \lesssim 20$ regime, agreeing with the results of numerical evolution within a few percent. In Ref.[3], this estimate was used, extrapolating it to large q. However, very recent numerical results for different families of profiles [13] indicate that the q-approach no longer holds in the high curvature regime. In this work we confirm a similar behaviour by using the profiles (16b).

Instead of q, we will use the dimensionless curvature of the linearized estimator $g(r)$ at its maximum, defined as,

$$w \equiv -r_m^2 \partial_r^2 g(r_m) = 4q C_c(q) \sqrt{1 - \frac{3}{2} C_c(q)}, \tag{21}$$

(see Eq. (58) of [10] for a derivation of the last relation), so that the q-approach prediction for the threshold $g_c(w)$ is given by [10],

$$g_c(w) = \frac{4}{3} \left(1 - \sqrt{1 - \frac{3}{2} C_c(q(w))} \right). \tag{22}$$

In the family of profiles (16b) a larger size r_m implies a larger dimensionless curvature w. Figure 1 shows the threshold values $g_c(w)$ we have obtained from numerical evolution for different lengthscales r_m. Note that the q-approach, given by Eqs. (20) and (22), underestimates the thresholds in the high-curvature regime, and that the numerical values enter the Type II region for $w \gtrsim 43$. This is in qualitative agreement with the results of [13].

VII. PBH ABUNDANCE

The study of threshold values for different families of primordial perturbation profiles provides a better understanding of the PBH abundance, since only perturbations with initial $g(r_m) > g_c$ will contribute. For quantitative estimates, we must now introduce the statistical framework for initial conditions. Following [10], the initial g is assumed to be a Gaussian random field, constrained to the following three conditions:

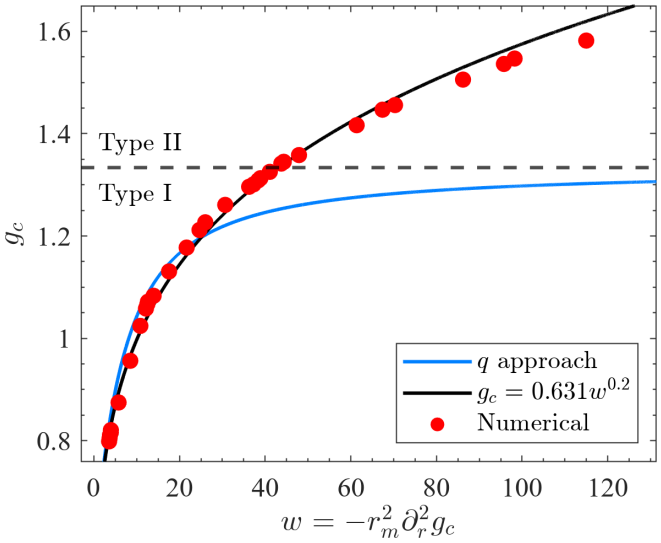

FIG. 1. Threshold values $g_c = g(r_m, \mu_c)$ and their dependence with the normalized curvature around its maximum, $\omega = -r_m^2 \partial_r^2 g_c(r_m)$, comparing the q-approach prediction with the numerical results, fitted using a power-law scaling curve, $g_c(w) = 0.631 w^{0.2}$, with deviations only up to 3% for the values of w studied. The case shown corresponds to a scale hierarchy of $\alpha \equiv k_{\rm UV}/k_{\rm IR} = 25$.

1. Noting that high peaks of a Gaussian random field are nearly spherically symmetric [11], we require that there is a spatial point $\vec{x} = \vec{x}_p$ around which C has a peak as a function of $\vec{x}$, i.e $\vec{\nabla} C(r, \vec{x})\big|_{\vec{x}=\vec{x}_p} = 0$, with $\nabla^2 C(r, \vec{x})\big|_{\vec{x}=\vec{x}_p} < 0$. Here $r = \|\vec{x} - \vec{x}_p\|$ is the comoving distance to the center of symmetry.

2. We require $C(r, \vec{x}_p)$ to have a maximum at $r = r_m$.

3. We require $C(r_m, \vec{x}_p) \geq C_c$.

From these three conditions, and within the statistical framework of peak theory [11], a formula for the abundance of PBH was obtained in [10]. Such formula considered only Type I black holes, neglecting the contribution of Type II to the total abundance. Note that, for Type II conditions, corresponding to $g(r_m) > 4/3$, the maximum of g transforms into a local minimum of C, so the second condition cannot be implemented. The non-monotonic behavior of C with g will also make the third condition unphysical, since black holes will form for $g > g_c$, which means $C < C_c$. A simple way to include Type II black holes in the expression for the total abundance, which we adopt here, is to express these three conditions in terms of the variable g, and then integrate g from the threshold to arbitrarily large values. The formula for the total abundance of PBH is similar to the one obtained in [10], with the difference that Type II will also be included. Following the discussion of [10], the density of "peaks" located at $\vec{x} = \vec{x}_p$, constrained to have a maximum value of g at $r = \|\vec{x} - \vec{x}_p\| = r_m$ is

$$\frac{dn_{\rm peaks|r_m}}{dr} = \sum_{\vec{x}_p, r_m} \delta(\vec{x} - \vec{x}_p)\delta(r - r_m), \tag{23}$$

where it is assumed that a peak and a maximum of g does not happen at more than one smoothing scale, which is indeed reasonable for the profiles studied numerically. Integrating over the location $\vec{x}_p$ of the peaks appropriately, and over the location of the maximum r_m,[10], a formula for the density of peaks of given size $r = r_m$ can be derived. This results in the following expression for the contribution of PBH to the present cold dark matter density parameter $\Omega_{\rm PBH}$, including both Type I and Type II, [2]

$$\Omega_{\rm PBH} = \int_{r_{\rm min}}^{r_{\rm eq}} d\log r \int_0^\infty w\, dw \tag{24}$$

$$\int_{g_c(w)}^\infty dg \frac{M(r,g,w)}{M_H(r)} \frac{4\pi r_{\rm eq}}{3r} \frac{f(\chi/\sigma_\chi) p(g, w, v=0)}{(2\pi/3)^{3/2}(\sigma_1/\sigma_2)^3}. \tag{25}$$

Here, and in what follows, we have dropped the subindex m in r_m, so r is the lengthscale at which we condition the profile $g(r)$ to have its maximum We also have $w \equiv -r^2\partial_r^2 g$ and $v \equiv r\partial_r g$, while $\chi \equiv -r^2\nabla^2 g_r = 2g + w$ is the trace of the Hessian around the peak. The function $f(x)$ comes from a phase space integration over the traceless part of the Hessian, at the position $\vec{x}_p$ of the peak's center [3], and is given by the following expression [11],

$$f(x) \equiv \frac{x^3 - 3x}{2}\left[\text{erf}\left(\sqrt{\frac{5}{2}}x\right) + \text{erf}\left(\sqrt{\frac{5}{2}}\frac{x}{2}\right)\right] + \tag{26}$$

$$\sqrt{\frac{2}{5\pi}}\left[\left(\frac{31x^2}{4} + \frac{8}{5}\right)e^{-5x^2/8} + \left(\frac{x^2}{2} - \frac{8}{5}\right)e^{-5x^2/2}\right].$$

$r_{\rm min}$ is the minimum lengthscale of a black hole that has not yet been evaporated, and $r_{\rm eq} = H_{\rm eq}^{-1}$ is the horizon size at matter radiation equality [10]. The probability distribution $p(g, w, v = 0)$ is given by,

$$p(g, w, v = 0) = \frac{p(g, w)}{\sqrt{2\pi\sigma_v^2}}, \tag{27}$$

where the distribution of v is Gaussian, centered at $v = 0$, and the joint distribution of w and g is bivariate Gaussian. Setting $\sigma_x^2 \equiv \langle x^2\rangle$, $\sigma_{xy}^2 \equiv \langle xy\rangle$, $\gamma_{xy} \equiv \frac{\sigma_{xy}^2}{\sigma_x\sigma_y}$, and defining $\tilde{\sigma}_x^2 = \sigma_x^2(1 - \gamma_{vx}^2)$, and $\tilde{\sigma}_{wg}^2 = \sigma_{wg}^2 - \frac{\sigma_{wv}^2\sigma_{vg}^2}{\sigma_v^2}$ then the joint distribution can be explicitly written as [3],

$$p(g, w) = \mathcal{N}(g|0, \tilde{\sigma}_g^2)\mathcal{N}(w|\bar{w}, \tilde{\sigma}_w^2(1 - \tilde{\gamma}^2)), \tag{28}$$

[2] In [3], the integral in g is performed only up to $g = 4/3$. Another difference is in the expression of the mass M, which here is assumed to have critical scaling with g, not C.

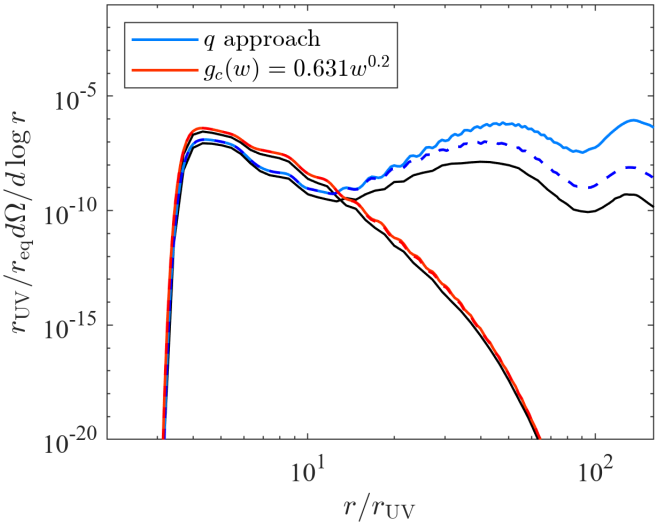

FIG. 2. Abundance of PBH per $\log r$, for the q approach prediction and for the numerical power law fit $g_c(w)$. Dashed lines correspond to the same abundance considering only Type I, and the black lines correspond to a critical scaling of the type $M \propto (C - C_c)^\gamma$, as done in [3], considering also Type I only. The curves shown correspond to $A_s = 0.01$ and $\alpha \equiv k_{\rm UV}/k_{\rm IR} = k_{\rm UV} r_{\rm IR} = 25$.

where $\tilde{\gamma} = \tilde{\sigma}_{wg}^2/(\tilde{\sigma}_w\tilde{\sigma}_g)$ and $\bar{w} \equiv \tilde{\gamma}(\tilde{\sigma}_w/\tilde{\sigma}_g)g$. The above correlators are integrals over the power spectrum $P_\zeta(k)$ defined in (17), and can all be expressed (see [10]) in terms of the momenta σ_j, defined as

$$\sigma_j^2 \equiv \frac{16}{81}\int d\log k (kr)^{4+2j} W^2(kr) P_\zeta(k), \qquad (29)$$

for $j = 0, 1, 2$, where $W(x) \equiv 3(\sin x - x\cos x)x^{-3}$. Finally, for the mass of the PBH we assume the critical scaling [6]

$$M(r, g, w) = \mathcal{K} M_H(r)(g - g_c(w))^\gamma, \qquad (30)$$

with $\gamma \approx 0.36$. For illustrative purposes we assume the fiducial value $\mathcal{K} = 6$ for the prefactor. Here, $M_H(r) \propto r^2$ is the mass of radiation within a Hubble radius when the comoving scale r falls within the horizon.

The results for the abundance (25) per logarithmic interval of r are displayed in Figure 2. The results from numerical evolution are compared with the q-approach predictions. This comparison raises questions about the *unexpected shape* of the PBH mass function found in [3], with a second peak of the mass function at the infrared scale $k_{\rm UV}\, r \sim \alpha$. May this be an artifact due to the use of the q-approach estimate for $g_c(w)$? With the power law fit to $g_c(w)$ which is obtained from the numerical evolution of our one-parameter family of profiles (we recall that these are motivated by the primordial power spectrum (17) and the 3 conditions displayed in Section VII), the infrared peak does not appear.

VIII. CONCLUSIONS

In this paper, we have considered the time evolution of a one parameter family of initial overdensity profiles, given by (16b). This is motivated by a broad power spectrum of the form (17), and the condition that the linearized smoothed density contrast $g(r)$ has a high peak well above its root mean square at some scale r_m. Within this family, a larger value of r_m corresponds to a larger value of the dimensionless curvature $w = -r_m^2\partial_r^2 g_c$. We find $g_c(w) \sim 0.631w^{0.2}$ to be a good fit to the values obtained from numerical evolution of our profiles. The abundance of PBH per logarithmic interval of r, based on this new fit, is compared with the results of [3], which were based on the the q-approach. This raises the question of whether the unexpected infrared peak found in [3] may perhaps be an artifact due to extrapolation of the $q-$approach to very large w. Further work is needed in order to assess the true form of the mass function in the infrared regime. This might require integration over a more generic set of initial overdensity profiles.

Acknowledgments

I am grateful to Jaume Garriga for advice and guidance, to Albert Escrivà for introducing me to his numerical code and to J. Fumagalli, C. Germani and R. Sheth for comments. Finally, I would like to thank my parents and friends for their unconditional support and love.

[1] S. Hawking, Mon. Not. R. Astron. Soc. **152**, 75 (1971).
[2] B. Carr, K. Kohri, Y. Sendouda, and J. Yokoyama, Reports on Progress in Physics **84**, 116902 (2021).
[3] J. Fumagalli, J. Garriga, C. Germani, and R. K. Sheth, Phys. Rev. D **111**, 123518 (2025), URL `https://link.aps.org/doi/10.1103/k75n-3qz4`.
[4] C. W. Misner and D. H. Sharp, Phys. Rev. **136**, B571 (1964).
[5] A. Escrivà, Phys. Dark Univ. **27**, 100466 (2020).
[6] A. Escrivà, arXiv preprint arXiv:2504.05813 (2025).
[7] I. Musco, Phys. Rev. D **100**, 123524 (2019).
[8] M. Shibata and M. Sasaki, Phys. Rev. D **60**, 084002 (1999).
[9] V. Atal, J. Cid, A. Escrivà, and J. Garriga, J. Cosmol. Astropart. Phys. **2020**, 022 (2020).
[10] C. Germani and R. K. Sheth, Universe **9**, 421 (2023).
[11] J. M. Bardeen, J. Bond, N. Kaiser, and A. Szalay, Astrophysical Journal, Part 1 (ISSN 0004-637X), vol. 304. **304**, 15 (1986).
[12] A. Escrivà, C. Germani, and R. K. Sheth, Physical Review D **101**, 044022 (2020).
[13] A. Escrivà, arXiv preprint arXiv:2504.05814 (2025).

Abundància de forats negres primordials a partir de l'espectre de potència de pertorbacions cosmològiques

Author: Matteo Gabriel Marrone, mmarroma10@alumnes.ub.edu
Facultat de Física, Universitat de Barcelona, Diagonal 645, 08028 Barcelona, Spain.

Advisor: Jaume Garriga Torres, jgarriga@fqa.ub.edu

Resum: Un camp aleatori de pertorbacions cosmològiques pot tenir pics alts i rars que evolucionen de manera no lineal després de creuar l'horitzó durant l'era dominada per la radiació, formant forats negres primordials (PBH). Utilitzant resultats recents per a les estadístiques de grans sobredensitats inicials, considerarem una família de perfils ben motivats per a aquestes sobredensitats, determinant l'amplitud crítica que fa que col·lapsin gravitacionalment. Això és rellevant per determinar l'abundància de PBH per a un espectre de potència de pertorbacions cosmològiques determinat.
Paraules clau: Cosmologia, perturbacions primordials, col·lapse gravitacional, forats negres.
ODSs: Aquest TFG està relacionat amb els Objectius de Desenvolupament Sostenible (SDGs) següents:

OBJECTIUS DE DESENVOLUPAMENT SOSTENIBLE (ODSS O SDGS)

1. Fi de la es desigualtats		10. Reducció de les desigualtats	
2. Fam zero		11. Ciutats i comunitats sostenibles	
3. Salut i benestar		12. Consum i producció responsables	
4. Educació de qualitat	X	13. Acció climàtica	
5. Igualtat de gènere		14. Vida submarina	
6. Aigua neta i sanejament		15. Vida terrestre	
7. Energia neta i sostenible		16. Pau, justícia i institucions sòlides	
8. Treball digne i creixement econòmic		17. Aliança pels objectius	
9. Indústria, innovació, infraestructures			

El contingut d'aquest TFG, part d'un grau universitari de Física, es relaciona amb l'ODS 4 ja que contribueix a l'educació de qualitat a nivell universitari.